PHASE-FIELD MODELING OF PRESSURIZED FRACTURES IN A POROELASTIC MEDIUM *

ANDRO MIKELIĆ* , MARY F. WHEELER† , AND THOMAS WICK †

Abstract. In this paper we present an incremental formulation of the phase field model for a fluid filled crack in a poroelastic medium. The mathematical model represents a linear elasticity system with fading elastic moduli as the crack grows that is coupled with an elliptic variational inequality for the phase field variable. The convex constraint of the variational inequality assures the irreversibility and entropy compatibility of the crack formation. We establish existence of a minimizer of an energy functional of an incremental problem and convergence of a finite dimensional approximation. Computational results of benchmark problems are provided that demonstrate the effectiveness of this approach in treating fracture propagation.

Keywords Hydraulic fracturing, Phase field formulation, Nonlinear elliptic system, Computer simulations, Poroelasticity

AMS classcode 35Q74; 35J87; 49J45; 65K15; 74R10

1. Introduction. The coupling of flow and geomechanics in porous media is a major research topic in energy and environmental modeling. Of specific interest is induced hydraulic fracturing or hydrofracturing commonly known as fracking. This technique is used to release petroleum and natural gas that includes shale gas, tight gas, and coal seam gas for extraction. Here fracking creates fractures from a wellbore drilled into reservoir rock formations. In 2012, more than one million fracturing jobs were performed on oil and gas wells in the United States and this number continues to grow. Clearly there are economic benefits of extracting vast amounts of formerly inaccessible hydrocarbons. In addition, there are environmental benefits of producing natural gas, much of which is produced in the United States from fracking. Opponents to fracking point to environmental impacts such as contamination of ground water, risks to air quality, migration of fracturing chemical and surface contamination from spills to name a few. For these reason, hydraulic fracturing is being heavily scrutinized resulting in the need for accurate and robust mathematical and computational models for treating fluid field fractures surrounded by a poroelastic medium.

Even in the most basic formulation, hydraulic fracturing is complicated to model since it involves the coupling of (i) mechanical deformation; (ii) the flow of fluids within the fracture and in the reservoir; (iii) fracture propagation. Generally, rock deformation is modeled using the theory of linear elasticity which can be represented by an integral equation that determines a relationship between fracture width and the fluid pressure. Fluid flow in the fracture is modeled using lubrication theory that relates fluid flow velocity, fracture width and the gradient of pressure. Fluid flow in the reservoir is modeled as a Darcy flow and the respective fluids are coupled through a leakage term. The criterion for fracture propagation is usually given by the conventional energy-release rate approach of linear elastic fracture mechanics (LEFM)

*A.M. would like to thank *Institute for Computational Engineering and Science (ICES)*, UT Austin for hospitality during his sabbatical stay from February to July, 2013. The research by M. F. Wheeler was partially supported by the U.S. Department of Energy, Office of Science, Office of Basic Energy Sciences through *DOE Energy Frontier Research Center: The Center for Frontiers of Subsurface Energy Security (CFSES)* under Contract No. DE-FG02-04ER25617, MOD. 005.

*Université de Lyon, CNRS UMR 5208, Université Lyon 1, Institut Camille Jordan, 43, blvd. du 11 novembre 1918, 69622 Villeurbanne Cedex, France

†Center for Subsurface Modeling, The Institute for Computational Engineering and Sciences, The University of Texas at Austin, Austin, Texas 78712, USA

theory; that is the fracture propagates if the stress intensity factor at the tip matches the rock toughness. Detailed discussion of the development of hydraulic fracturing models for use in petroleum engineering can be found in [1] and in mechanical engineering and hydrology in [25], [8], [17] and in references therein.

Major difficulties in simulating hydraulic fracturing in a deformable porous medium are treating crack propagation induced by high-pressure slick water injection and later the coupling to a multiphase reservoir simulator for production. A computational effective procedure in modeling coupled multiphase flow and geomechanics is to apply an iterative coupling algorithm as described in [21] and [22]. In the following, we briefly recapitulate this approach:

Iterative coupling is a sequential procedure where either the flow or the mechanics is solved first followed by solving the other problem using the latest solution information. At each time step the procedure is iterated until the solution converges within an acceptable tolerance. There are four well-known iterative coupling procedures and we are interested primarily in one referred to as the fixed stress split iterative method.

In order to fix ideas we address the simplest model of real applied importance, namely, the quasi-static single phase Biot system. Let $\mathcal{C}$ denote any open set homeomorphic to an ellipsoid in $\mathbb{R}^3$ (a crack set). Its boundary is a closed surface $\partial\mathcal{C}$. In most applications $\mathcal{C}$ is a curved 3D domain, with two dimensions significantly smaller than the dominant one. Nevertheless, we consider $\mathcal{C}$ as a 3D domain and use its particular geometry only when discussing the stress interface conditions. We notice that in many references on fracture propagation, the crack $\mathcal{C}$ is considered as a lower dimensional manifold and the lubrication theory is applied to describe the fluid flow (see e.g. [1] and [15]). We recall that the 3D flow in $\mathcal{C}$ can be reconstructed from a lower dimensional lubrication approximation (see [24]). The quasi-static Biot equations (see e.g. [28]) are an elliptic-parabolic system of PDEs, valid in the poroelastic domain $\Omega = (0, L)^3 \setminus \overline{\mathcal{C}}$, where for every $t \in (0, T)$ we have

$$\sigma^{por} - \sigma_0 = \mathcal{G}e(\mathbf{u}) - \alpha p I; \quad -\text{ div } \{\sigma^{por}\} = \rho_b \mathbf{g}; \tag{1.1}$$

$$\partial_t\big(\frac{1}{M}p + \text{ div } (\alpha\mathbf{u})\big) + \text{ div } \{\frac{\mathcal{K}}{\eta}(\rho_f \mathbf{g} - \nabla p)\} = f, \tag{1.2}$$

where σ_0 is the reference state total stress. Here, the boundary of $(0, L)^3$ is denoted by $\partial\Omega = \partial_D\Omega \cup \partial_N\Omega$ divided into Dirichlet and Neumann parts, respectively. We assume that meas$(\partial_D\Omega) > 0$. Boundary conditions on $\partial\Omega = \partial_D\Omega \cup \partial_N\Omega$ for the above situation involve displacements and traction as well as pressure and flux.

SYMBOL	*QUANTITY*	*UNITY*
$\mathbf{u}$	displacement	m
p	fluid pressure	Pa
σ^{por}	total poroelasticity tensor	Pa
$e(\mathbf{u}) = (\nabla\mathbf{u} + \nabla^\tau\mathbf{u})/2$	linearized strain tensor	dimensionless
$\mathcal{K}$	permeability	Darcy
α	Biot's coefficient	dimensionless
ρ_b	bulk density	kg/m^3
η	fluid viscosity	$kg/$m sec
M	Biot's modulus	Pa
$\mathcal{G}$	Gassman rank-4 tensor	Pa

TABLE 1.1
Unknowns and effective coefficients

The important parameters and unknowns are given in the Table 1.1.

The *fixed stress split* iterative method consists in imposing constant volumetric mean total stress σ_v. This means that the $\sigma_v = \sigma_{v,0} + K_{dr}\ \mathrm{div}\ \mathbf{u}I - \alpha pI$ is kept constant at the half-time step. The iterative process reads as follows:

$$\left(\frac{1}{M} + \frac{\alpha^2}{K_{dr}}\right)\partial_t p^{n+1} + \ \mathrm{div}\ \{\frac{\mathcal{K}}{\eta}(\rho_f \mathbf{g} - \nabla p^{n+1})\} =$$

$$-\frac{\alpha}{K_{dr}}\partial_t \sigma_v^n + f = f - \alpha\ \mathrm{div}\ \partial_t \mathbf{u}^n + \frac{\alpha^2}{K_{dr}}\partial_t p^n; \tag{1.3}$$

$$-\ \mathrm{div}\ \{\mathcal{G}e(\mathbf{u}^{n+1})\} + \alpha\nabla p^{n+1} = 0. \tag{1.4}$$

REMARK 1. *We remark that the fixed stress approach is useful in employing existing reservoir simulators in that (1.3) can be extended to treat the mass balance equations arising in black oil or compositional flows and allows decoupling of multi-phase flow and elasticity.*

REMARK 2. *Interest in the system (1.3)-(1.4) is based on its robust numerical convergence. Under mild hypothesis on the data, the convergence of the iterations was studied in [21] and it was proven that the solution operator $\mathcal{S}$, mapping $\{\mathbf{u}^n, p^n\}$ to $\{\mathbf{u}^{n+1}, p^{n+1}\}$ is a contraction on appropriate functional spaces with contraction constant $\gamma_{FS} = \dfrac{M\alpha^2}{K_{dr} + M\alpha^2} < 1$. The corresponding unique fixed point satisfies equations (1.1)-(1.2).*

Focus on crack propagation in the fixed-stress elasticity step
Because of the complexity of this coupled nonlinear fluid-mechanics system, we follow the above splitting strategy and restrict our attention to a simplified model in which we assume the pressure has been computed from the previous fixed-stress fluid iteration step. Our focus in this paper is therefore on crack **propagation** in the framework of the fixed-stress mechanics step (1.4) and we call this approach **pressurized crack surrounded by a poroelastic medium**.

REMARK 3. *The extension to the full poroelastic system for crack propagation and therefore employing a phase-field formulation of* (1.3) *is beyond the scope of this paper. The latter method is called* ***fluid-filled crack propagation*** *in a poroelastic medium and we refer the reader to [24].*

In the following, we present an incremental formulation of the pressurized crack surrounded by a poroelastic medium. The mathematical model involves the coupling of a linear elasticity system with an elliptic variational inequality for the phase field variable. With this approach, branching of fractures and heterogeneities in mechanical properties can be effectively treated as demonstrated numerically in Section 5.

Our formulation follows Miehe et al. in [19] and is a thermodynamically consistent framework for phase-field models of quasi-static crack propagation in elastic solids, together with incremental variational principles. This work is based on the variational approach to elastic fractures by Francfort and Marigo ([13] and [5]). Our methodology represents an extension to cracks in a poroelastic medium containing a viscous fluid. Recently, numerical phase field experiments of a pressurized quasi-static brittle fracture were undertaken in [29] employing our phase-field model, as well as in [7] using the method presented in [5].

Following Griffith's criterion, we suppose that the crack propagation occurs when the elastic energy restitution rate reaches its critical value G_c. If τ is the traction force applied at the part of the boundary $\partial_N\Omega$, then we associate to the crack $\mathcal{C}$ the

following total energy

$$E(\mathbf{u},\mathcal{C}) = \int_\Omega \frac{1}{2}\mathcal{G}e(\mathbf{u}) : e(\mathbf{u})\ dx - \int_{\partial_N\Omega} \tau\cdot\mathbf{u}\ dS - \int_\Omega \alpha p_B \mathrm{div}\ \mathbf{u}\ dx + G_c\mathcal{H}^2(\mathcal{C}),\ (1.5)$$

where p_B is the poroelastic medium pressure calculated in the previous iterative coupling step and $\alpha \in (0,1)$ is the Biot coefficient.

This energy functional is then minimized with respect to the kinematically admissible displacements $\mathbf{u}$ and any crack set satisfying a crack growth condition. The computational modeling of this minimization problem treats complex crack topologies and requires approximation of the crack location and of its length. This is overcome by regularizing the sharp crack surface topology in the solid by diffusive crack zones described by a scalar auxiliary variable. This variable is a phase-field that interpolates between the unbroken and the broken states of the material.

The model proposed in this paper is a basic one that can be analyzed both as a minimization and as a variational PDE formulation. For simplicity the presentation here is based on energy minimization whereas our treatment of the corresponding variational formulation can be found in [23]. In the numerical analysis of fracture propagation in solid mechanics, solving the minimization problem by considering the variational formulation is treated in [9]. Here we have chosen our computational framework to be based on the variational formulation since more additional realistic physical interface effects (see Fig. 2.1 and [1]) and associated dissipative terms and nonlinear physical models can be employed.

The outline of our paper is as follows: In Section 2, we introduce an incremental formulation of a phase-field model for a pressurized crack. Here, the crack-pressure is incorporated with an interface law. In Section 3, we present a mathematical analysis of the incremental problem. In Section 4, a numerical formulation is briefly described. Finally in Section 5 we provide numerical experiments for classical benchmark cases, e.g. Sneddon's pressurized crack with constant fluid pressure (see Subsection 5.2 and [26]).

2. An incremental phase field formulation. We introduce the time-dependent crack phase field φ, defined on $(0,L)^3 \times (0,T)$. The regularized crack functional reads

$$\Gamma_\varepsilon(\varphi) = \int_{(0,L)^3} (\frac{1}{2\varepsilon}(1-\varphi)^2 + \frac{\varepsilon}{2}|\nabla\varphi|^2)\ dx = \int_{(0,L)^3} \gamma(\varphi,\nabla\varphi)\ dx, \qquad (2.1)$$

where γ is the crack surface density per unit volume. This regularization of $\mathcal{H}^2(\mathcal{C})$, in the sense of the $\Gamma-$limit when $\varepsilon \to 0$, was used in [4].

Our further considerations are based on the fact that evolution of cracks is fully dissipative in nature. First, the crack phase field φ is intuitively a regularization of $1 - \mathbb{1}_{\mathcal{C}}$ and we impose its negative evolution

$$\partial_t\varphi \le 0. \qquad (2.2)$$

Next we follow [19] and [7] and replace energy (1.5) by a global constitutive dissipation functional for a rate independent fracture process. That is

$$E_\varepsilon(\mathbf{u},\varphi) = \int_{(0,L)^3} \frac{1}{2}\big((1-k)\varphi^2 + k\big)\mathcal{G}e(\mathbf{u}) : e(\mathbf{u})\ dx - \int_{\partial_N\Omega} \tau\cdot\mathbf{u}\ dS -$$
$$\int_{(0,L)^3} \alpha\varphi^{1+b} p_B \mathrm{div}\ \mathbf{u}\ dx + G_c \int_{(0,L)^3} \left(\frac{1}{2\varepsilon}(1-\varphi)^2 + \frac{\varepsilon}{2}|\nabla\varphi|^2\right) dx,\ b \ge 0. \qquad (2.3)$$

where b is a fixed nonnegative constant and k is a positive regularization parameter for elastic energy, with $k \ll \varepsilon$. We note that the pressure cross term reads $\int_{(0,L)^3} \alpha\varphi^{1+b} p_B \text{div } \mathbf{u} dx$ instead of $\int_{(0,L)^3} \alpha\varphi p_B \text{div } \mathbf{u} dx$. This is linked to the behavior for negative values of the phase field. If $\varphi \leq 0$, then there should be no contribution. Therefore instead of $\int_{(0,L)^3} \alpha\varphi p_B \text{div } \mathbf{u}\ dx$, we should have $\int_{(0,L)^3} \alpha\varphi_+ p_B \text{div } \mathbf{u}\ dx$. However, this functional is not C^1 and would lead to complications in numerical simulations. For $0 \leq \varphi \leq 1$, using φ_+^{1+b}, $b \geq 0$, instead of φ_+ in the pressure cross term should not affect the phase field approximation. If $\varphi = \mathbb{1}_{\mathcal{C}}$, we do not see any difference. In summary, adding $b > 0$ is a way to avoid difficulties linked to the lack of smoothness.

In the following, we consider a quasi-static formulation where velocity changes are small. First, we derive an incremental form, i.e., we replace the time derivative in inequality (2.2) with a discretized version; more precisely

$$\partial_t \varphi \to \partial_{\Delta t} \varphi = (\varphi - \varphi_p)/(\Delta t),$$

where $\Delta t > 0$ is the time step and φ_p is the phase field from the previous time step. After time discretization, our quasistatic constrained minimization problem becomes a stationary problem, called the incremental problem.

Second, the crack is pressurized and the energy E_ε given by (2.3) is incomplete; we next model the crack-pressure based on an interface law. A general description of a crack embedded in a porous medium is illustrated in Figure 2.1. Here, we consider a simplified situation in which the complex interface crack/pore structure is neglected. We notice that such a complex structure would require the solution of a variational problem since the formulation as energy minimization might not be well defined. Furthermore, we assume that the crack is a 3D thin domain with width much less than length, then lubrication theory can be applied. Hence, the leading order of the stress in $\mathcal{C}$ is $-p_f I$. At the crack boundary we have the continuity of the contact force, which yields

$$\sigma \mathbf{n} = (\mathcal{G}e(\mathbf{u}) - \alpha p_B I)\mathbf{n} = -p_f \mathbf{n}, \tag{2.4}$$

where p_f denotes the fracture pressure and $\mathbf{n}$ the normal vector.

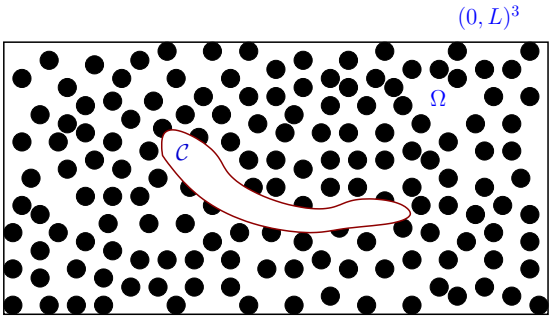

FIG. 2.1. *A crack $\mathcal{C}$ embedded in a porous medium. Here, the dimensions of the crack are assumed to be much larger than the pore scale size (black dots) of the porous medium.*

Before introducing the phase field, we eliminate the traction crack surface integrals

and obtain

$$\int_\Omega \alpha p_B \text{div } \mathbf{w}\ dx + \int_{\partial\mathcal{C}} \sigma\mathbf{n}\mathbf{w}\ dS = \int_\Omega \alpha p_B \text{div } \mathbf{w}\ dx - \int_{\partial\mathcal{C}} p_f w_n\ dS =$$
$$\int_\Omega \alpha p_B \text{div } \mathbf{w}\ dx - \int_\Omega \text{div } (p_B\mathbf{w})\ dx + \int_{\partial_N\Omega} p_B w_n\ dS = \int_\Omega (\alpha-1) p_B \text{div } \mathbf{w}\ dx -$$
$$\int_\Omega \nabla p_B \mathbf{w}\ dx + \int_{\partial_N\Omega} p_B w_n\ dS,$$

where w_n denotes the normal component of the vector function w.

REMARK 4. *In the previous calculations, the first line reads*

$$\int_\Omega \alpha p_B div\ \mathbf{w}\ dx + \int_{\partial\mathcal{C}} \sigma\mathbf{n}\mathbf{w}\ dS = \int_\Omega \alpha p_B div\ \mathbf{w}\ dx - \int_{\partial\mathcal{C}} p_f w_{n,poroelastic}\ dS.$$

Setting now $p = p_f$ in the crack and $p = p_B$ in the poroelastic medium, then the above calculations yield

$$\int_\Omega \alpha p_B div\ \mathbf{w}\ dx - \int_{\partial\mathcal{C}} p_f w_{n,poroelastic}\ dS = \int_{(0,L)^3} \alpha p div\ \mathbf{w}\ dx +$$
$$\int_{\mathcal{C}} \nabla p\mathbf{w}\ dx - \int_{\mathcal{C}} div\ (p\mathbf{w})\ dx - \int_{\partial\mathcal{C}} p_f w_{n,poroelastic}\ dS =$$
$$\int_{(0,L)^3} \alpha p div\ \mathbf{w}\ dx + \int_{\mathcal{C}} \nabla p\mathbf{w}\ dx - \int_{\partial\mathcal{C}} p(w_{n,poroelastic} - w_{n,crack})\ dS.$$

The last term coincides with the virtual work of the pressure force as introduced in [10] and applied in [7]. In the above calculations, surface integrals are now treated with Gauss' divergence theorem:

$$-\int_{\partial_N\Omega} \tau\cdot\mathbf{w}\ dS + \int_{\partial\mathcal{C}} p w_n\ dS - \int_\Omega \alpha p \text{ div } \mathbf{w}\ dx = -\int_\Omega (\alpha-1) p \text{ div } \mathbf{w}\ dx +$$
$$\int_\Omega \nabla p\mathbf{w}\ dx - \int_\Omega \text{ div } (\mathcal{T}\mathbf{w})\ dx = -\int_\Omega (\alpha-1) p \text{ div } \mathbf{w}\ dx +$$
$$\int_\Omega (\nabla p - \text{ div } \mathcal{T})\mathbf{w}\ dx - \int_\Omega \mathcal{T} : e(\mathbf{w})\ dx, \tag{2.5}$$

where $\mathcal{T}$ is a smooth symmetric 3×3 matrix with compact support in a neighborhood of $\partial(0,L)^3$, such that $\mathcal{T}\mathbf{n} = \tau + p\mathbf{n}$ on $\partial_N(0,L)^3$. The tensor $\mathcal{T}$ is introduced in order to handle the phase field only in volume terms. Supposing that the crack $\mathcal{C}$ does not interact with $\partial_N\Omega$, it can be eliminated by using Green's formula. Hence the solution does not depend on the choice of $\mathcal{T}$. We set

$$\mathcal{F} = -(\alpha-1)pI - \mathcal{T}, \qquad \mathbf{f} = \nabla p - \text{ div } \mathcal{T}. \tag{2.6}$$

After the above transformations, we have the following variant of the energy functional (2.3):

$$\tilde{E}_\varepsilon(\mathbf{u},\varphi) = \int_{(0,L)^3} \frac{1}{2}\big((1-k)\varphi^2 + k\big)\mathcal{G}e(\mathbf{u}) : e(\mathbf{u})\ dx + \int_{(0,L)^3} \varphi^{1+b}(\mathcal{F} : e(\mathbf{u}) +$$
$$\mathbf{f}\cdot\mathbf{u})\ dx + G_c \int_{(0,L)^3} \left(\frac{1}{2\varepsilon}(1-\varphi)^2 + \frac{\varepsilon}{2}|\nabla\varphi|^2\right) dx,\ b \geq 0. \tag{2.7}$$

In the case of elastic cracks it can be shown that the phase field unknown satisfies $0 \leq \varphi \leq 1$. In order to establish this property for the spatially continuous incremental problem, we first modify (2.7) for negative values of φ. We now use φ_+ instead of φ in terms where negative φ could lead to incorrect physics in the bulk energy, traction and pressure forces. With this modification, the final energy functional reads

$$\mathcal{E}_\varepsilon(\mathbf{u},\varphi) = \int_{(0,L)^3} \frac{1}{2}\big((1-k)\varphi_+^2 + k\big)\mathcal{G}e(\mathbf{u}) : e(\mathbf{u})\; dx + \int_{(0,L)^3} \varphi_+^{1+b}(\mathcal{F} : e(\mathbf{u}) + \mathbf{f}\cdot\mathbf{u})\; dx + G_c \int_{(0,L)^3} \left(\frac{1}{2\varepsilon}(1-\varphi)^2 + \frac{\varepsilon}{2}|\nabla\varphi|^2\right) dx,\ b \geq 0. \tag{2.8}$$

As functional space of admissible displacements, we choose

$$V_U = \{\mathbf{z} \in H^1((0,L)^3)^3 \mid \mathbf{z} = 0 \text{ on } \partial_D\Omega\ \}.$$

The entropy condition (2.2) is imposed in its discretized form and we introduce a convex set K:

$$K = \{\psi \in H^1((0,L)^3) \mid \psi \leq \varphi_p \leq 1 \text{ a.e. on } (0,L)^3\}, \tag{2.9}$$

where $\varphi_p(x)$ is the value of the phase field from the previous time step. The incremental minimization problem now reads

DEFINITION 2.1. *Find $\mathbf{u} \in V_U$ and a nonnegative $\varphi \in K$ such that*

$$\mathcal{E}_\varepsilon(\mathbf{u},\varphi) = \min_{\{\mathbf{v},\psi\}\in V_U\times K} \mathcal{E}_\varepsilon(\mathbf{v},\psi). \tag{2.10}$$

Note that the value of the phase field unknown φ from the previous time step enters only the convex set K, as the obstacle φ_p. The goal of the next section is to establish a solution to the minimization problem (2.10).

REMARK 5. *For $b > 0$, the corresponding Euler-Lagrange equations read*

$$-\ div\left(\big((1-k)\varphi_+^2 + k\big)\mathcal{G}e(\mathbf{u})\right) + \varphi_+^{1+b}\mathbf{f} - \ div\,(\varphi_+^{1+b}\mathcal{F}) = 0 \quad in \quad (0,L)^3, \tag{2.11}$$

$$\mathbf{u} = 0 \quad on \quad \partial_D(0,L)^3, \tag{2.12}$$

$$\big((1-k)\varphi_+^2 + k\big)\mathcal{G}e(\mathbf{u})\mathbf{n} = -\varphi_+^{1+b}\mathcal{F}\mathbf{n} \quad on \quad \partial_N(0,L)^3, \tag{2.13}$$

$$\partial_{\Delta t}\varphi \leq 0 \quad on \quad (0,L)^3 \quad and \quad \frac{\partial\varphi}{\partial\mathbf{n}} = 0 \quad on \quad \partial(0,L)^3; \tag{2.14}$$

$$-G_c\varepsilon\Delta\varphi - \frac{G_c}{\varepsilon}(1-\varphi) + (1-k)\mathcal{G}e(\mathbf{u}) : e(\mathbf{u})\varphi_+ + (1+b)\varphi_+^b(\mathcal{F} : e(\mathbf{u}) + \mathbf{f}\cdot\mathbf{u}) \leq 0 \quad in \quad (0,L)^3, \tag{2.15}$$

$$\Big\{-G_c\varepsilon\Delta\varphi - \frac{G_c}{\varepsilon}(1-\varphi) + (1-k)\mathcal{G}e(\mathbf{u}) : e(\mathbf{u})\varphi_+ + (1+b)\varphi_+^b(\mathcal{F} : e(\mathbf{u}) + \mathbf{f}\cdot\mathbf{u})\Big\}\partial_{\Delta t}\varphi = 0 \ \ in \ \ (0,L)^3, \tag{2.16}$$

where (2.16) *is the strong form of Rice' condition.* This two-field formulation can be compared with the Model I formulation given in [19] (see page 1289). The main difference is that the system (2.11)-(2.16) is a variational inequality; and in [19] a penalization term is used for solving the inequality.

3. Well-posedness of the model.

3.1. Existence of a minimizer to the energy functional $\mathcal{E}_\varepsilon$. In this section, we seek for a solution to the minimization problem (2.10). The strategy is to consider the integrand of (2.8), using the notation $\mathbf{z} := (\mathbf{v}, \phi)$, and ξ stands for the components of the gradient of the displacements and the gradient of the phase-field function. With z_4, we access the fourth component of $\mathbf{z}$, namely the phase-field function. Lastly, z_{4+} denotes the positive part of the phase-field unknown. Then,

$$g(x,\mathbf{z},\xi) = \frac{1}{2}\big((1-k)(\inf\{z_{4+},1\})^2+k\big)\sum_{i,j,k,r=1}^{3}\mathcal{G}_{ijkr}\xi_{kr}\xi_{ij} + G_c(\frac{1}{2\varepsilon}(1-z_4)^2+ \frac{\varepsilon}{2}|\nabla z_4|^2) + (\inf\{z_{4+},1\})^{1+b}(\sum_{i,j=1}^{3}F_{ij}\xi_{ij}+\sum_{i=1}^{3}f_i z_i), \tag{3.1}$$

defined on $(0,L)^3\times\mathbb{R}^4\times\mathbb{R}^{12}\to\mathbb{R}\cup\{+\infty\}$. It is convex in ξ and we will prove that it is

(i) a Caratheodory function (i.e. a continuous function on $\mathbb{R}^4\times\mathbb{R}^{12}$ for every x from $(0,L)^3$ and a measurable function on $(0,L)^3$ for every $\{\mathbf{z},\xi\}$ from $\mathbb{R}^4\times\mathbb{R}^{12}$);

(ii) the energy functional (2.8) is coercive.

Then Corollary 3.24, page 97, from Dacorogna's monograph [11] yields the lower semi-continuity of the energy functional. Proving existence of at least one point of minimum is then classical.

We start with a result which follows directly from the basic theory:

LEMMA 3.1. *Let $\mathbf{f}$ and $\mathbf{F}\in L^2$; and G_c, b be nonnegative constants. Let ε be a positive small parameter. Then the integrand g given by (3.1) is a Caratheodory function.*

PROPOSITION 3.2. *Under the assumptions of Lemma 3.1, the functional*

$$\Phi(\mathbf{v},\phi) = \int_{(0,L)^3} g(x,\{\mathbf{v},\phi\},\{e(\mathbf{v}),\nabla\phi\})\,dx \tag{3.2}$$

is coercive over $V_U\times H^1((0,L)^3)\cap K$, i.e.

$$\lim\Phi(\mathbf{v},\phi)\to\infty, \qquad \textit{when} \quad ||\mathbf{v}||_{V_U}+||\phi||_{H^1}\to\infty. \tag{3.3}$$

Proof. Let us introduce the abbreviation $\tilde{\phi} = \inf\{\phi_+,1\}$. Let c be a generic constant. We estimate all terms one by one:

$$|\int_{(0,L)^3}(\tilde{\phi})^{b+1}(\mathbf{f}\cdot\mathbf{v}+\mathcal{F}:e(\mathbf{v})\,dx| \le ||\mathbf{v}||_{L^2}\,||\mathbf{f}||_{L^2}+||\tilde{\phi}e(\mathbf{v})||_{L^2}\,||\mathcal{F}||_{L^2}. \tag{3.4}$$

The elastic energy terms yields

$$\int_{(0,L)^3}\big((1-k)(\tilde{\phi})^2+k\big)\mathcal{G}e(\mathbf{v}):e(\mathbf{v})\,dx \ge ck||e(\mathbf{v})||^2_{L^2}+c(1-k)||\tilde{\phi}e(\mathbf{v})||^2_{L^2}. \tag{3.5}$$

We recall that, by Korn's inequality,

$$||\mathbf{v}||_{H^1((0,L)^3)}\le C_K||e(\mathbf{v})||_{L^2((0,L)^3)}, \qquad \forall\mathbf{v}\in V_U. \tag{3.6}$$

Therefore, putting together (3.4) and (3.5), and using (3.6), yields

$$\Phi(\mathbf{v},\phi) \geq G_c \int_{(0,L)^3} \Big(\frac{(1-\phi)^2}{2\varepsilon}+\varepsilon|\nabla\phi|^2\Big)\ dx + \frac{ck}{4}||e(\mathbf{v})||^2_{L^2}+ \\ \frac{c(1-k)}{4}||\tilde{\phi}e(\mathbf{v})||^2_{L^2} - \frac{||\mathcal{F}||^2_{L^2}}{c(1-k)} - \frac{C_K^2||\mathbf{f}||^2_{L^2}}{ck}. \tag{3.7}$$

The coerciveness property (3.3) follows from (3.7). □

Our goal is to prove the following theorem:

THEOREM 3.3. *(Existence of a minimizer to the incremental phase field problem) Let $\varepsilon, k > 0$, $b \geq 0$ and $\mathcal{F}$, $\mathbf{f} \in L^2$, $\varphi_p \in H^1$, $0 \leq \varphi_p \leq 1$ a.e. on $(0,L)^3$. Then the minimization problem (2.10) has at least one solution $\{\mathbf{u},\varphi\} \in V_U \times K$ and $\varphi \geq 0$ a.e. on $(0,L)^3$.*

Proof. (of Theorem 3.3) Let $\{\mathbf{u}^k,\varphi^k\}_{k\in\mathbb{N}} \in V_U \times K$ be a minimizing sequence for the minimization problem (2.10) for Φ; that is a sequence of elements of $V_U \times K$ such that $\Phi(\mathbf{u}^k,\varphi^k) \to \inf_{V_U\times K}\Phi(\mathbf{v},\phi)$. By proposition (3.2) and the inequality (3.7) $\inf_{V_U\times K}\Phi(\mathbf{v},\phi) \neq -\infty$. The sequence $\{\mathbf{u}^k,\varphi^k\}_{k\in\mathbb{N}}$ is uniformly bounded in $V_U \times K$ and $\{\varphi^k_+\}_{k\in\mathbb{N}}$ is uniformly bounded in $L^\infty((0,L)^3)$. Therefore there exists $\{\mathbf{u},\varphi\}$ and a subsequence, denoted by the same superscript, such that for $k \to \infty$

$$\{\mathbf{u}^k,\varphi^k\} \to \{\mathbf{u},\varphi\} \quad \text{weakly in } V_U \times H^1((0,L)^3), \quad \text{strongly in } \ L^q((0,L)^3)^4,\ q<6, \\ \text{and a.e. on} \quad (0,L)^3. \tag{3.8}$$

Next, the inequality (3.7) yields

$$g(x,\mathbf{v},\xi) \geq < a(x),\xi > + B, \qquad \{\mathbf{v},\xi\} \in \mathbb{R}^4 \times \mathbb{R}^{12} \quad \text{and a.e.} \quad x \in (0,L)^3,$$

with $a \in L^2$ and $B \in \mathbb{R}$. Consequently, we are in situation to apply Corollary 3.24, page 97, from [11]. It yields the weak lower semicontinuity of the functional Φ and hence

$$\Phi(\mathbf{u},\varphi) \leq \liminf \Phi(\mathbf{u}^k,\varphi^k) = \inf_{V_U\times K}\Phi(\mathbf{v},\phi). \tag{3.9}$$

Hence $\{\mathbf{u},\varphi\} \in V_U \times H^1((0,L)^3) \cap K$ is a solution for the minimization problem.

It remains to prove that φ is nonnegative. We evaluate the functional Φ at the point $\{\mathbf{u},\varphi_+\}$. Obviously $\varphi_+ \in K$. A direct calculation yields

$$\Phi(\mathbf{u},\varphi_+) = \Phi(\mathbf{u},\varphi) - \frac{G_c}{2\varepsilon}\int_{(0,L)^3}\varphi_-(\varphi_- - 2)\ dx - \frac{\varepsilon G_C}{2}\int_{(0,L)^3}|\nabla\varphi_-|^2\ dx. \tag{3.10}$$

Therefore $\{\mathbf{u},\varphi\}$ can be a point of minimum only if $\varphi_- = 0$ and we conclude that $\varphi \geq 0$ a.e. on $(0,L)^3$. □

COROLLARY 3.4. *Let the hypotheses of Theorem 3.3 be satisfied and $b > 0$. Then the Euler-Lagrange equations corresponding to the minimization problem (2.10)*

$$\int_{(0,L)^3} (1-k)\varphi\psi\mathcal{G}e(\mathbf{u}) : e(\mathbf{u})\ dx + G_c \int_{(0,L)^3} \big(-\frac{1}{\varepsilon}(1-\varphi)\psi + \varepsilon\nabla\varphi\cdot\nabla\psi\big)\ dx$$

$$+(1+b)\int_{(0,L)^3} \varphi^b(\mathbf{f}\cdot\mathbf{u} + \mathcal{F} : e(\mathbf{u}))\psi\, dx \le 0,\ \forall\psi \in H^1((0,L)^3),\ \psi \ge 0\ \textit{a.e. on}\ (0,L)^3, \tag{3.11}$$

$$\int_{(0,L)^3} (1-k)\varphi(\varphi_p-\varphi)\mathcal{G}e(\mathbf{u}) : e(\mathbf{u})\ dx + G_c \int_{(0,L)^3} \big(-\frac{1}{\varepsilon}(1-\varphi)(\varphi_p-\varphi) +$$

$$\varepsilon\nabla\varphi\cdot\nabla(\varphi_p-\varphi)\big)\ dx + (1+b)\int_{(0,L)^3} \varphi^b(\mathbf{f}\cdot\mathbf{u} + \mathcal{F} : e(\mathbf{u}))(\varphi_p-\varphi)\ dx = 0. \tag{3.12}$$

$$\int_{(0,L)^3} \big((1-k)\varphi^2 + k\big)\mathcal{G}e(\mathbf{u}) : e(\mathbf{w})\ dx + \int_{(0,L)^3} \varphi^{b+1}(\mathcal{F} : e(\mathbf{w}) + \mathbf{f}\cdot\mathbf{w})\ dx = 0,\ \forall\mathbf{w} \in V_U. \tag{3.13}$$

admit a solution $\{\mathbf{u},\varphi\} \in V_U \times H^1((0,L)^3) \cap K$, such that $\varphi \ge 0$ a.e. on $(0,L)^3$. We observe that equation (3.12) is the Rice condition (see e.g. [14]).

3.2. A finite dimensional approximation. Let $\{\psi_r\}_{r\in\mathbb{N}}$ be a smooth basis for $H^1((0,L)^3)$ and $\{\mathbf{w}^r\}_{r\in\mathbb{N}}$ be a smooth basis for V_U. We start by defining a finite dimensional approximation to the minimization problem (2.10).

DEFINITION 3.5 (**of a penalized approximation**). *Let us suppose the assumptions of Theorem 3.3 and a penalization parameter $\delta \in \mathbb{R}$ and in particular, let $\delta := M \in \mathbb{N}$ in this section. Let $\tilde{\varphi} = \inf\{1, \varphi_+\}$. The pair $\{\mathbf{u}^M, \varphi^M\}$, $\mathbf{u}^M = \sum_{r=1}^M a_r\mathbf{w}^r$ and $\varphi^M = \sum_{r=1}^M b_r\psi_r$, is a finite dimensional approximative solution for problem (2.10) if it is a minimizer to the problem*

$$\inf_{V_U^M \times W^M} \{\Phi(\mathbf{v},\phi) + \int_{(0,L)^3} \frac{\delta}{2}(\phi - \varphi_p^M)_+^2\ dx\}, \tag{3.14}$$

where $V_U^M = span\ \{\mathbf{w}^r\}_{r=1,\dots,M}$, $W^M = span\ \{\psi_r\}_{r=1,\dots,M}$ and φ_p^M is a projection of φ_p on W^M.

REMARK 6. *For $b > 0$, every solution for the problem (3.14) satisfies the discrete variational formulation*

$$\int_{(0,L)^3} \big((1-k)(\tilde{\varphi}^M)^2 + k\big)\mathcal{G}e(\mathbf{u}^M) : e(\mathbf{w}^r)\ dx +$$

$$\int_{(0,L)^3} (\tilde{\varphi}^M)^{b+1}(\mathcal{F} : e(\mathbf{w}^r) + \mathbf{f}\cdot\mathbf{w}^r)\ dx = 0, \quad \forall r = 1,\dots,M, \tag{3.15}$$

$$G_c\int_{(0,L)^3} \big(-\frac{1}{\varepsilon}(1-\varphi^M)\psi_r + \varepsilon\nabla\varphi^M\cdot\nabla\psi_r\big)\ dx + \int_{(0,L)^3} \delta(\varphi^M - \varphi_p^M)_+\psi_r\ dx +$$

$$(1+b)\int_{(0,L)^3} (\tilde{\varphi}^M)^b(\mathcal{F} : e(\mathbf{u}^M) + \mathbf{f}\cdot\mathbf{u}^M)\psi_r\ dx +$$

$$\int_{(0,L)^3} (1-k)\tilde{\varphi}^M\psi_r\mathcal{G}e(\mathbf{u}^M) : e(\mathbf{u}^M)\ dx = 0, \quad \forall\ r = 1,\dots,M. \tag{3.16}$$

PROPOSITION 3.6. *We assume the hypotheses of Theorem 3.3 and $b > 0$. Then there exists a penalized finite dimensional approximation for problem (3.14) that satisfies the a priori estimate*

$$G_c \int_{(0,L)^3} \frac{(1-\varphi^M)^2}{\varepsilon}\, dx + \int_{(0,L)^3} M(\varphi^M - \varphi_p^M)_+^2\, dx + k||e(\mathbf{u}^M)||_{L^2}^2 + ||\tilde{\varphi}^M e(\mathbf{u}^M)||_{L^2}^2 \leq c, \tag{3.17}$$

where c is independent of M, k and ε.

Proof. This is a consequence of (3.7) in Proposition (3.2) and the continuity of the integrand. □

THEOREM 3.7. *Assume the hypotheses of Theorem 3.3 and let $b > 0$. Then there exists a subsequence of $\{\mathbf{u}^M, \varphi^M\} \in V_U^M \times W^M$, denoted by the same symbol, and $\{\mathbf{u}, \varphi\} \in V_U \times H^1((0,L)^3) \cap K$, $\varphi \geq 0$ a.e., being a minimizer to the problem (2.10) and such that*

$$\{\mathbf{u}^M, \varphi^M\} \to \{\mathbf{u}, \varphi\} \quad in \quad V_U \times H^1((0,L)^3). \tag{3.18}$$

Proof. (of Theorem 3.7) By Proposition 3.6 there is a solution $\{\mathbf{u}^M, \varphi^M\}$ for problem (3.14), satisfying a priori estimate (3.17). Therefore there exists $\{\mathbf{u}, \varphi\}$ and a subsequence, denoted by the same superscript, such that

$$\begin{gathered}\{\mathbf{u}^M, \varphi^M\} \to \{\mathbf{u}, \varphi\} \quad \text{weakly in } V_U \times H^1((0,L)^3), \\ \text{strongly in } \; L^q((0,L)^3)^4,\ q < 6, \quad \text{and a.e. on} \quad (0,L)^3, \quad \text{as} \quad M \to \infty.\end{gathered} \tag{3.19}$$

Obviously $(\varphi^M - \varphi_p^M)_+ \to 0$, as $M \to \infty$, and $\varphi \in K$.

Next, let $\phi \in K^N = \{z \in W^N : z(x) \leq \varphi_p^M(x) \text{ a.e. on } (0,L)^3\}, N \leq M$. Then we have

$$\Phi(\mathbf{u}^M, \varphi^M) + \int_{(0,L)^3} \frac{M}{2}(\varphi^M - \varphi_p^M)_+^2\, dx \leq \Phi(\mathbf{v}, \phi), \quad \forall \{\mathbf{v}, \phi\} \in V_U^N \times W^N \cap K.$$

and the limit $M \to \infty$ yields

$$\Phi(\mathbf{u}, \phi) \leq \Phi(\mathbf{v}, \phi), \quad \forall \{\mathbf{v}, \phi\} \in V_U^N \times W^N \cap K.$$

After passing to the limit $N \to \infty$, we conclude that $\{\mathbf{u}, \varphi\} \in V_U \times H^1((0,L)^3) \cap K$ is a solution to problem (2.10). As before, it still can be shown that φ is nonnegative.

It remains to establish strong convergence of the gradients.

Passing to the limit in equation (3.15) is straightforward and we conclude that $\{\mathbf{u}, \varphi\}$ satisfies equation (3.13). Next we choose $\mathbf{w} = \mathbf{u}^M$ as test function in (3.15) and pass to the limit $M \to \infty$. Thus,

$$\int_{(0,L)^3} \big((1-k)(\varphi_+)^2 + k\big)\mathcal{G}e(\mathbf{u}) : e(\mathbf{u})\, dx + \int_{(0,L)^3} (\varphi_+)^{b+1}(\mathcal{F} : e(\mathbf{u}) + \mathbf{f} \cdot \mathbf{u})\, dx = 0. \tag{3.20}$$

Therefore we have the convergence of the weighted elastic energies

$$\lim_{M\to\infty}\int_{(0,L)^3}\big((1-k)(\tilde{\varphi}^M)^2+k\big)\mathcal{G}e(\mathbf{u}^M):e(\mathbf{u}^M)\ dx=$$
$$\int_{(0,L)^3}\big((1-k)(\varphi_+)^2+k\big)\mathcal{G}e(\mathbf{u}):e(\mathbf{u})\ dx. \tag{3.21}$$

Using Fatou's lemma we have

$$\int_{(0,L)^3}\liminf_{M\to\infty}\big((1-k)(\tilde{\varphi}^M)^2+k\big)\mathcal{G}e(\mathbf{u}^M):e(\mathbf{u}^M)\ dx$$
$$\leq\liminf_{M\to\infty}\int_{(0,L)^3}\big((1-k)(\tilde{\varphi}^M)^2+k\big)\mathcal{G}e(\mathbf{u}^M):e(\mathbf{u}^M)\ dx$$
$$=\int_{(0,L)^3}\big((1-k)(\varphi_+)^2+k\big)\mathcal{G}e(\mathbf{u}):e(\mathbf{u})\ dx. \tag{3.22}$$

Consequently

$$\mathbf{u}^M\to\mathbf{u}\quad\text{strongly in}\quad V_U,\quad\text{as}\ \ M\to\infty. \tag{3.23}$$

For every $\psi\in L^\infty((0,L)^3)\cap H^1((0,L)^3)$, (3.23) implies

$$\lim_{M\to\infty}|\int_{(0,L)^3}\tilde{\varphi}^M\psi\mathcal{G}e(\mathbf{u}^M-\mathbf{u}):e(\mathbf{u}^M-\mathbf{u})\ dx|\to 0,\quad\text{as}\ \ M\to\infty,$$

and

$$\int_{(0,L)^3}\tilde{\varphi}^M\psi\mathcal{G}e(\mathbf{u}^M):e(\mathbf{u}^M)\ dx=\int_{(0,L)^3}\tilde{\varphi}^M\psi\mathcal{G}e(\mathbf{u}^M-\mathbf{u}):e(\mathbf{u}^M-\mathbf{u})\ dx+$$
$$2\int_{(0,L)^3}\tilde{\varphi}^M\psi\mathcal{G}e(\mathbf{u}^M):e(\mathbf{u})\ dx-\int_{(0,L)^3}\tilde{\varphi}^M\psi\mathcal{G}e(\mathbf{u}):e(\mathbf{u})\ dx\to$$
$$\int_{(0,L)^3}\varphi_+\psi\mathcal{G}e(\mathbf{u}):e(\mathbf{u})\ dx,\quad\text{as}\ \ M\to\infty. \tag{3.24}$$

Next we use Minty's lemma and write equation (3.16) in the equivalent form

$$\int_{(0,L)^3}(1-k)\inf\{\varphi_+^M,1\}(\psi-\varphi^M)\mathcal{G}e(\mathbf{u}^M):e(\mathbf{u}^M)\ dx+G_c\int_{(0,L)^3}\big(\frac{(\psi-1)}{\varepsilon}(\psi-\varphi^M)$$
$$+\varepsilon\nabla\psi\cdot\nabla(\psi-\varphi^M)\big)dx+(1+b)\int_{(0,L)^3}(\inf\{\varphi_+^M,1\})^b\ (\mathbf{f}\cdot\mathbf{u}^M+\mathcal{F}:e(\mathbf{u}^M))(\psi-\varphi^M)dx$$
$$+\int_{(0,L)^3}M(\psi-\varphi_p^M)_+(\psi-\varphi^M)\ dx\geq 0,\quad\forall\ \psi\in W^M. \tag{3.25}$$

After taking $\psi=\varphi_p^M$, we use the convergence (3.24) pass to the limit $M\to\infty$ (see e. g. [18]), and obtain

$$\lim_{M\to\infty}G_c\int_{(0,L)^3}\varepsilon|\nabla\varphi^M|^2\ dx=-\int_{(0,L)^3}(1-k)\varphi(\varphi-\varphi_p)\mathcal{G}e(\mathbf{u}):e(\mathbf{u})\ dx+$$
$$\int_{(0,L)^3}\big(\frac{G_c}{\varepsilon}(1-\varphi_p)(\varphi-\varphi_p)-\frac{G_c}{\varepsilon}(\varphi-\varphi_p)^2+\varepsilon\nabla\varphi\cdot\nabla\varphi_p\big)\ dx-$$
$$(1+b)\int_{(0,L)^3}\varphi^b\ (\mathbf{f}\cdot\mathbf{u}+\mathcal{F}:e(\mathbf{u}))(\varphi-\varphi_p)\ dx=G_c\int_{(0,L)^3}\varepsilon|\nabla\varphi|^2\ dx. \tag{3.26}$$

□

4. Numerical approximation. We now formulate finite element approximations to (3.11) - (3.13), which are analogous to equations (3.15)–(3.16). For spatial discretization, we apply a standard Galerkin finite element method on quadrilaterals. Specifically, we approximate displacements by continuous bilinears and refer to the finite element space as V_h. Also, we take φ to be bilinears in order to assure continuity, and denote this space as W_h. Here h represents the standard approximation parameter. In this section, we present the discretization of our phase-field formulation;

$$\int_{(0,L)^3} \big((1-k)(\tilde{\varphi}^h)^2 + k\big)\mathcal{G}e(\mathbf{u}^h) : e(\mathbf{w})\ dx +$$

$$\int_{(0,L)^3} (\tilde{\varphi}^h)^{b+1}(\mathcal{F} : e(\mathbf{w}) + \mathbf{f}\cdot\mathbf{w})\ dx = 0 \quad \forall \mathbf{w} \in V_h, \tag{4.1}$$

$$G_c \int_{(0,L)^3} \Big(-\frac{1}{\varepsilon}(1-\varphi^h)\psi + \varepsilon\nabla\varphi^h\cdot\nabla\psi\Big)\ dx + \int_{(0,L)^3} \delta(\partial_{\Delta t}\varphi^h)_+\psi\ dx +$$

$$(1+b)\int_{(0,L)^3} (\tilde{\varphi}^h)^b(\mathcal{F} : e(\mathbf{u}^h) + \mathbf{f}\cdot\mathbf{u}^h)\psi\ dx +$$

$$\int_{(0,L)^3} (1-k)\tilde{\varphi}^h\psi\mathcal{G}e(\mathbf{u}^h) : e(\mathbf{u}^h)\ dx = 0 \quad \forall\ \psi \in W_h, \tag{4.2}$$

with $b > 0$. In our numerical examples presented in this paper, we note that $\mathcal{T} \equiv 0$ because the applied forces are either Dirichlet displacement conditions or specified pressure p_B. Then, the terms in (2.6) for $\mathcal{F}$ and $\mathbf{f}$ reduce to $\mathcal{F} = -(\alpha-1)pI$ and $\mathbf{f} = \nabla p$.

The incremental formulation (4.1)-(4.2) corresponds to the (pseudo-) time stepping scheme based on a difference quotient approximation with backward differences for the time derivatives. In the quasi-static model the time derivative $\delta[\partial_t\varphi]_+$ is present and is discretized as follows

$$\delta[\partial_t\varphi]_+ \to \delta[\partial_{\Delta t}\varphi]_+ = \delta\frac{[\varphi - \varphi^{n-1}]_+}{\Delta t},$$

with the time step size Δt, where $n-1$ is used to indicate the preceding time step. We then obtain for the weak form:

$$\delta(\varphi_+ - \varphi_+^{n-1}, \psi)_{L^2} + \Delta t(B,\psi)_{L^2} = 0, \quad \forall\psi \in W_h. \tag{4.3}$$

Here, $(\cdot,\cdot)$ denotes the discrete scalar product in L^2 and A and B denote the operators of all remaining terms for the present time step in the weak formulation, where the equation (4.3) is related to equations (4.1) and (4.2). Finally, the spatially discretized semi-linear form can be written in the following way:

FINITE ELEMENT FORMULATION 1. *Find* $\mathbf{U}^h := \{\mathbf{u}^h, \varphi^h\} \in V_h \times W_h$ *such that:*

$$A(\mathbf{U}^h)(\mathbf{\Psi}) = \delta([\varphi^h - \varphi^{h,n-1}]_+, \psi)_{L^2} + \Delta t A_S(\mathbf{U}^h)(\mathbf{\Psi}) = 0,$$

with

$$A_S(\mathbf{U}^h)(\mathbf{\Psi}) = \Big(((1-k)(\inf\{\varphi_+^h, 1\})^2 + k)\mathcal{G}e(\mathbf{u}^h), e(\mathbf{w})\Big)_{L^2} - \langle\tau, \mathbf{w}\rangle_{\partial_N\Omega}$$
$$- ((\inf\{\varphi_+^h, 1\})^{1+b}(\alpha-1)p_B, \nabla\cdot\mathbf{w})_{L^2} + (\nabla p_B(\inf\{\varphi_+^h, 1\})^{1+b}, \mathbf{w})_{L^2} +$$
$$\Big((1-k)\mathcal{G}e(\mathbf{u}^h) : e(\mathbf{u}^h)(\inf\{\varphi_+^h, 1\}), \psi\Big)_{L^2} - \frac{G_c}{\epsilon}(1-\varphi^h, \psi)_{L^2} + G_c\epsilon(\nabla\varphi^h, \nabla\psi)_{L^2}$$
$$- (1+b)\Big((\inf\{\varphi_+^h, 1\})^b\big((\alpha-1)p_B\nabla\cdot\mathbf{u}^h - \nabla p_B\cdot\mathbf{u}^h\big), \psi\Big)_{L^2} = 0,$$

for all $\mathbf{\Psi} = \{\mathbf{w}, \psi\} \in V_h \times W_h$*, where* $A_S(\cdot)(\cdot)$ *is the sum of equations* (4.1) *and* (4.2) *and equality* (2.5) *is applied in the relation between* τ *and* $\mathcal{T}$*. Later in the simulations we choose* $b = 1$ *since for* $0 < b < 1$ *could lead to numerical difficulties in computing the second derivative, i.e, the Jacobian.*

4.1. Linearization and Newton's method. The nonlinear problem is solved with Newton's method. For the iteration steps $m = 0, 1, 2, \ldots$, it holds:

$$A'(\mathbf{U}^{h,m})(\mathbf{\Delta U}^h, \mathbf{\Psi}) = -A(\mathbf{U}^{h,m})(\mathbf{\Psi}), \quad \mathbf{U}^{h,m+1} = \mathbf{U}^{h,m} + \lambda \mathbf{\Delta U}^h,$$

with $\mathbf{\Delta U}^h = \{\mathbf{\Delta u}^h, \Delta\varphi^h\}$, and a line search parameter $\lambda \in (0, 1]$. Here, we need the (approximated) Jacobian of Finite Element Formulation 1 (defined without using the subscript h):

$$A'(\mathbf{U})(\mathbf{\Delta U}, \mathbf{\Psi}) = \Big(\varphi_+ \Delta\mathbf{u}, \mathbf{w}\Big)_{L^2} + \delta(\Delta[\varphi - \varphi^{n-1}]_+, \psi)_{L^2} + \Delta t A'_S(\mathbf{U})(\mathbf{\Delta U}, \mathbf{\Psi}),$$

with

$$\begin{aligned}
A'_S(\mathbf{U})(\mathbf{\Delta U}, \mathbf{\Psi}) = \Big(&2(1-k)\inf\{\varphi_+, 1\}H(1-\varphi)\Delta\varphi\mathcal{G}e(\mathbf{u}) + ((1-k)(\inf\{\varphi_+, 1\})^2 \\
&+k)\mathcal{G}e(\Delta\mathbf{u}), e(\mathbf{w})\Big)_{L^2} - ((1+b)(\inf\{\varphi_+, 1\})^b H(1-\varphi)\Delta\varphi(\alpha-1)p_B, \nabla\cdot\mathbf{w})_{L^2} \\
&+((1+b)(\inf\{\varphi_+, 1\})^b H(1-\varphi)\Delta\varphi\nabla p_B, \mathbf{w})_{L^2} + \Big(2(1-k)\mathcal{G}e(\mathbf{u}) : e(\Delta\mathbf{u})\inf\{\varphi_+, 1\} \\
&+(1-k)\mathcal{G}e(\mathbf{u}) : e(\mathbf{u})H(1-\varphi)\Delta\varphi, \psi\Big)_{L^2} + \frac{G_c}{\epsilon}(\Delta\varphi, \psi)_{L^2} + G_c\epsilon(\nabla\Delta\varphi, \nabla\psi)_{L^2} - \\
&(\alpha-1)(1+b)(p_B(b(\inf\{\varphi_+, 1\})^{b-1}H(1-\varphi)\Delta\varphi\nabla\cdot\mathbf{u} + (\inf\{\varphi_+, 1\})^b\nabla\cdot\Delta\mathbf{u}), \psi)_{L^2} \\
&+(1+b)\Big(\nabla p_B\cdot(b(\inf\{\varphi_+, 1\})^{b-1}H(1-\varphi)\Delta\varphi\mathbf{u} + (\inf\{\varphi_+, 1\})^b\Delta\mathbf{u}), \psi\Big)_{L^2} = 0,
\end{aligned}$$

for all $\mathbf{\Psi} = \{\mathbf{w}, \psi\} \in V_h \times W_h$. $H(\cdot)$ is Heaviside's function.

REMARK 7. *Due to the nonconvexity of the energy functional* $\mathcal{E}_\varepsilon$*, the Jacobian matrix is indefinite. Therefore, in the numerical computations, we replace* φ^h *in the elasticity equation by a time-lagged* φ^h*, which has been demonstrated computationally to provide a robust and stable numerical scheme.*

5. Numerical Tests. We perform four different tests. In the first example, we neglect the pressure and reproduce benchmark results for crack growth in a pure (brittle) elastic regime with homogeneous material [20] and nonhomogeneous material. The second test assumes a constant pressure $p_B = 10^{-3}$ that is injected into the domain (Sneddon's 2d benchmark [27]). In the final example, we study two interacting propagating fracture subject to nonconstant pressure. The programming code is a modification of the multiphysics program template [30], based on the finite element software `deal.II` (see [2]).

5.1. Single edge notched tension test. In this first example, we compute the single edge notched tension test without using a pressure, i.e., $p_B = 0$. We use this test for code verification for benchmark tests in pure elasticity. The geometric and material properties are the same as used in [20]. The configuration is displayed in Figure 5.1. We use $\mu = 80.77kN/mm^2$, $\lambda = 121.15kN/mm^2$, and $G_c = 2.7N/mm$. The crack growth is driven by a non-homogeneous Dirichlet condition for the displacement field on Γ_{top}, the top boundary of Ω . We increase the displacement on Γ_{top} at each time step, namely

$$u_y = \Delta t \times \bar{u}, \quad \bar{u} = 1 \text{ mm}.$$

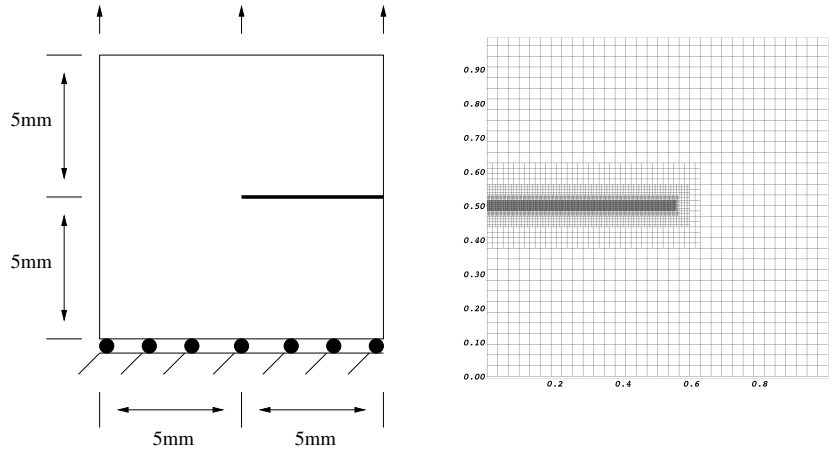

FIG. 5.1. *Example 1: Single edge notched tension test: configuration (left) and mesh. In detail, the boundary conditions are:* $u_y = 0$ *(homogeneous Dirichlet) and traction free in* x*-direction on the bottom. On the top boundary* Γ_{top}*, we prescribe* $u_x = 0$ *and* u_y *as provided in the text. All other boundaries including the slit are traction free (homogeneous Neumann conditions).*

Furthermore, we set $k = 10^{-10}$ and ε according to the theory of Γ-convergence; namely, $h = o(\varepsilon)$ with $\varepsilon = ch^{0.25}$ with $c = 0.125$. Computations are shown for three mesh levels $4+1, 4+2, 4+3$ (4 times global mesh refinement plus $1, 2, 3$ times local mesh refinement, respectively, in the region where we expect the crack to grow) in order to show the robustness and numerical stability of our approach. Here, $h = 0.022$ on $4+1$, $h = 0.011$ on $4+2$, and $h = 0.0056$ on $4+3$. The time step size is chosen 10^{-4} until time step 58 and is then switched to 10^{-6} (as suggested by Miehe et al. [20]). The penalization parameter is $\delta = 0$. We evaluate the surface load vector on the Γ_{top} as $\tau = (F_x, F_y)$,

where we are particularly interested in F_y as illustrated in Figure 5.2, we identify the same behavior for the load-displacement curve as observed in [20].

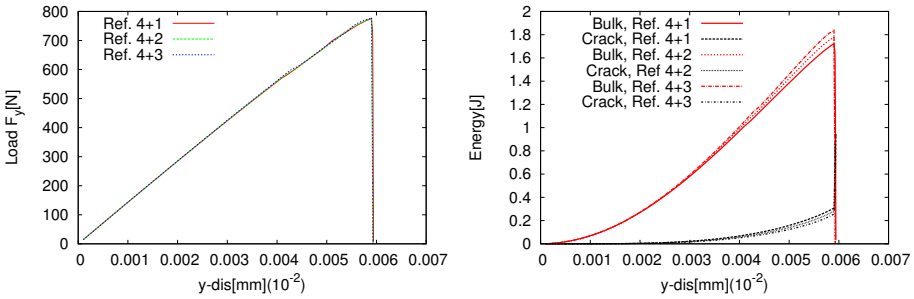

FIG. 5.2. *Example 1: Single edge notched tension test: load-displacement curves for different mesh levels (left) and evaluation of bulk and crack energies (right). The load-displacement curves are very close to Miehe et al. [20] and Borden's et al. [3] findings and in addition show the same evolution on different mesh levels, which indicates numerical robustness and stability of our approach. The energy evolutions confirm the theory that bulk energy is transformed into crack energy when the material is broken.*

In addition, we compute the bulk and crack energy respectively,

$$E_B = \int_\Omega ([1+\kappa]\varphi_+^2 + \kappa)\psi(e), \tag{5.1}$$

with the strain energy functional $\psi(e) := \mu tr(e(u)^2) + \frac{1}{2}\lambda tr(e(u))^2$, $e := e(u) := \frac{1}{2}(\nabla u + \nabla u^T)$. The crack energy is computed as

$$E_C = \frac{G_c}{2}\int_\Omega \Big(\frac{(\varphi-1)^2}{\varepsilon} + \varepsilon|\nabla\varphi|^2\Big)\,dx, \quad \text{with } |\nabla\varphi|^2 := \nabla\varphi : \nabla\varphi.$$

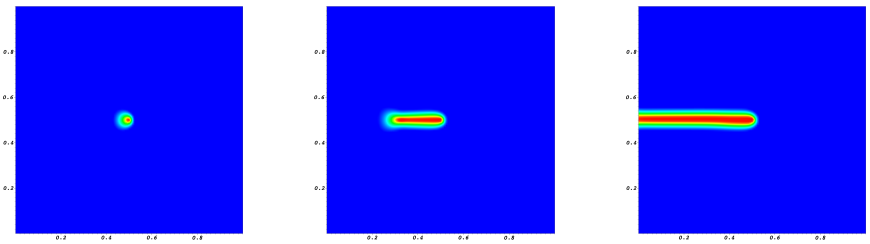

FIG. 5.3. *Example 1: Single edge notched tension test: crack pattern in red for three different displacement steps.*

In Figure 5.3, we identify the crack pattern for three different displacement steps.

We extend the previous configuration in order to demonstrate the performance of our approach. The distributed Lamé coefficients are used to simulate a heterogeneous material. Here, the regularization parameter ε is linked to the heterogeneities. In other words, as briefly described by [19], ε can be interpreted as a length-scale parameter that is linked to material properties. Nonhomogeneous material leads to non-planar and curvilinear crack-growths, branching and joining of cracks without any modifications in the program. The Lamé parameters are randomly distributed. The previous configuration is modified with respect to the geometry and the μ-λ-fields as displayed in Figure 5.4. Here, μ varies between $8.1 \times 10^4 - 5.8 \times 10^5$ and λ varies between $1.2 \times 10^5 - 6.2 \times 10^5$. All the other parameters remain the same as in the previous test. The load-displacement curve is observed in Figure 5.4. Finally, the crack path in this setting is shown in Figure 5.5.

5.2. Constant pressure in a crack (Sneddons's 2d benchmark). The second example is motivated by [7, 29] and is based on Sneddon's theoretical calculations [27, 26]. Specifically, we consider a 2D problem where a (constant) pressure p_B is used to drive the deformation and crack propagation. We assume a dimensionless form of the equations.

The configuration is displayed in Figure 5.6. We prescribe the initial crack implicitly (see e.g. Borden et al. [3]). Therefore, we deal with the following geometric data: $\Omega = (0,4)^2$ and a (prescribed) initial crack on the $y = 4.0$-line $\Omega_C = (1.8, 2.2) \subset \Omega$ with length $2l_0 = 0.4$. As boundary conditions we set the displacements zero on $\partial\Omega$. We perform two time steps since the test is stationary (a computational analysis has been performed in [29]).

Applying the theory of Γ-convergence based on a related finite element analysis in [6], we choose $h \ll k \ll \epsilon$, i.e., $k = 0.25\sqrt{h}$ and $\epsilon = 0.5\sqrt{h}$. Furthermore, it

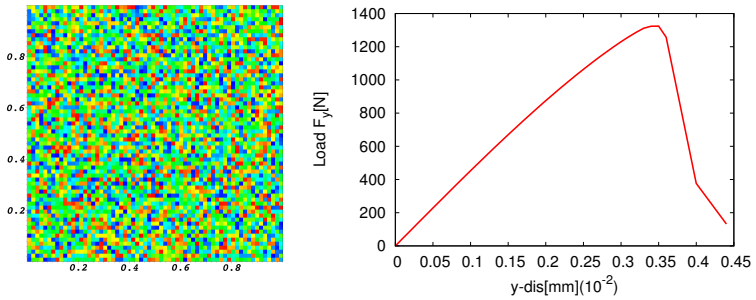

FIG. 5.4. *Example 1 with heterogeneous material: Geometry and μ-distribution at left. At right, the load-displacement curve is shown, which shows similar qualitative behavior as in the previous example without heterogeneities.*

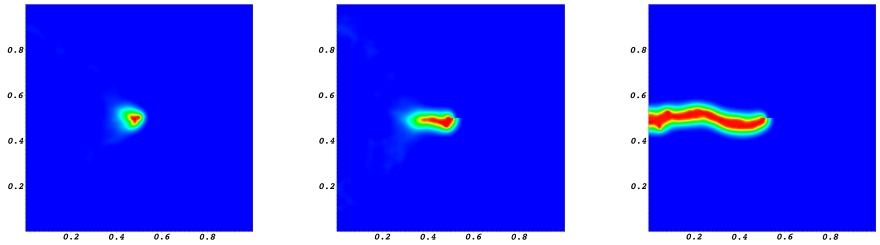

FIG. 5.5. *Example 1 with heterogeneous material: Crack path in red for three different time steps. As before the green color indicates the transition zone with $0 < \varphi < 1$.*

is well-known that δ must depend on h, i.e., here, we choose $\delta = 100 \times h^{-2}$. The Biot coefficient and critical energy release rate are chosen as $\alpha = 0$ and $G_c = 1.0$, respectively. The mechanical parameters are Young's modulus and Poisson's ratio are set to be $E = 1.0$ and $\nu_s = 0.2$. The injected pressure is $p_B = 10^{-3}$.

The goal is to measure the crack opening displacement (COD) and the volume of the crack under spatial mesh refinement. To do so, we observe u along Ω_C. Specifically, the width is determined as the jump of the normal displacements $w = COD = [\mathbf{u} \cdot \mathbf{n}]$. This expression can be written in integral form as follows:

$$w = COD = \int_{\infty}^{\infty} \mathbf{u} \cdot \nabla\varphi \, dy,$$

where φ is as before our phase-field function. We note that the integration is perpendicular to the crack direction. Here, the crack is aligned with the x-axis and therefore integration is along the y-direction. Second, following [12], p. 710, the volume of the fracture is $V = \pi w l_0$. The analytical expression for the width (to which we compare) [12] is $w = 4\frac{(1-\nu_s^2)l_0 p}{E}$. Then, the analytical expression for the volume becomes

$$V = 2\pi \frac{(1-\nu_s^2) l_0^2 p}{E}. \tag{5.2}$$

In contrast to [7], we use the numerical approximation of the phase-field function instead of a synthetic choice of the crack indicator function.

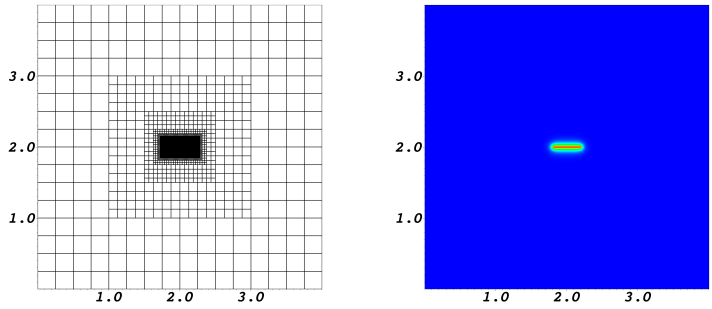

FIG. 5.6. *Example 2: Configuration (left) and crack pattern (right).*

The crack pattern and the corresponding mesh are displayed in Figure 5.6. Our findings for different spatial mesh parameters h are summarized in Figure 5.7. Specifically, we observe overall convergence to Sneddon's analytical solution [27] as well as much better approximation of the crack tips under mesh refinement. The obtained crack volumes are displayed in Table 5.1 in which the exact value is computed by Formula (5.2).

TABLE 5.1
Example 2: Fracture volume.

h	8.8×10^{-2}	4.4×10^{-2}	2.2×10^{-2}	1.1×10^{-2}	exact
V	3.02×10^{-4}	2.77×10^{-4}	2.57×10^{-4}	2.49×10^{-4}	2.41×10^{-4}

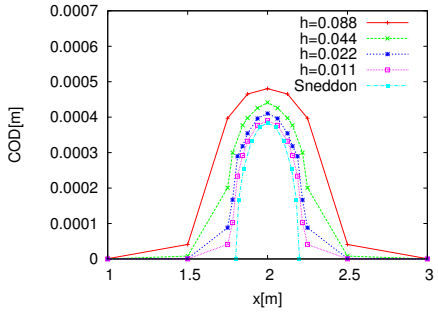

FIG. 5.7. *Example 2: COD for different h. Sneddon's turquoise line with squares corresponds to his analytical solution. It is well observed that the crack tips must be resolved correctly as they are not well approximated on coarse meshes.*

5.3. Two-crack interaction subject to non-constant pressure. In this final example, we extend the previous setting to study the interaction of two different fractures that are subject to a linearly increasing pressure p_B. In the first part, a homogeneous material is considered and in the second part a heterogenous material field. The pressure function is given by $p_B(t) = 0.1 + t \cdot 0.1$, where t denotes the total time, and Young's modulus is set to be $E = 1$ in the first part and it varies between

1.1 and 11.0 in the second part. Poisson ratio is 0.2. The penalization parameter is chosen as $\delta = 10h^{-2}$. The remaining parameters are chosen as in the previous examples. Our results in the Figures 5.8 and 5.9 show two propagating, interacting fractures. Specifically, they curve away due to stress-shadowing effects. The extension to nonconstant pressure evolution using Darcy's law and application of the fixed-stress splitting is studied in [31] and [24].

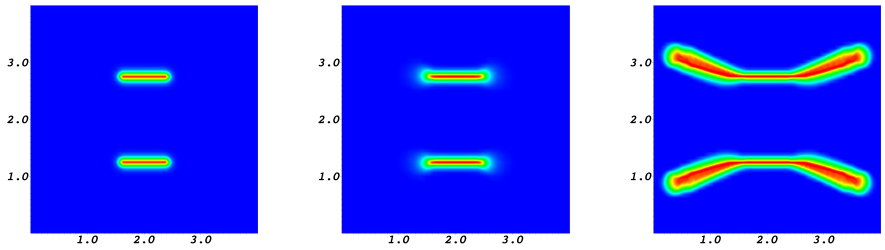

FIG. 5.8. *Example 3: crack evolution in red in a homogeneous material at times* $T = 0, 15, 30$.

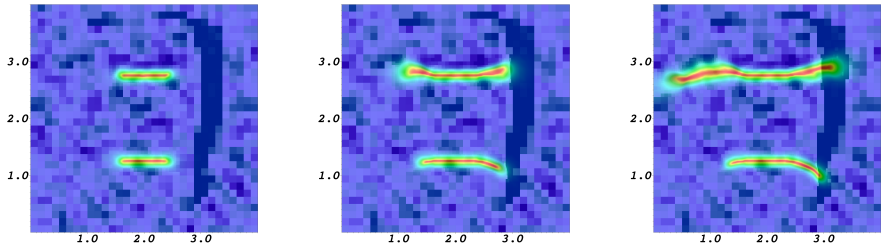

FIG. 5.9. *Example 3: crack evolution in red in a heterogeneous material at times* $T = 30, 40, 50$. *The light blue regions denote smooth material* $E \approx 1$ *and dark blue stands for* $E \approx 11.0$.

6. Conclusion. In this paper, we formulated a phase-field model for pressurized and propagating cracks in a poroelastic medium. The phase-field algorithm is based on an incremental formulation and existence of a minimizer is established. Numerical benchmarks are demonstrating the correctness of the theory. Specifically, this approach can treat crack growth in heterogeneous porous media and pressurized crack evolutions. Ongoing computations involve coupling this framework to a multiphase reservoir simulator for modeling hydraulic fracturing as well as treating intersecting fractures.

REFERENCES

[1] J. Adachi, E. Siebrits, A.Peirce, J. Desroches, Computer simulation of hydraulic fractures, International Journal of Rock Mechanics and Mining Sciences, Vol. 44 (2007), p. 739–757.
[2] W. Bangerth, T. Heister, G. Kanschat, Differential Equations Analysis Library, 2012.
[3] M. J. Borden, C. V. Verhoosel, M. A Scott, T. J. R. Hughes, C. M. Landis, A phase-field description of dynamic brittle fracture, Computer Methods in Applied Mechanics and Engineering, Vol. 217 (2012), p. 77-95.
[4] B. Bourdin, G.A. Francfort, J.-J. Marigo, Numerical experiments in revisited brittle fracture, J. Mech. Phys. Solids, 48 (4) (2000): 797–826.

[5] B. Bourdin, G.A. Francfort, J.-J. Marigo, The Variational Approach to Fracture, J. Elasticity 91 (1-3) (2008): 1–148.
[6] B. Bourdin, Image Segmentation with a finite element method, Mathematical Modelling and Numerical Analysis 33 (2) (1999): 229–244.
[7] B. Bourdin, C. Chukwudozie, K. Yoshioka, A Variational Approach to the Numerical Simulation of Hydraulic Fracturing, SPE Journal, Conference Paper 159154-MS, 2013.
[8] R. de Borst, J. Rethoré, M.A. Abellan, A numerical approach for arbitrary cracks in a fluid-saturated porous medium, Arch. Appl. Mech. 75 (2006) 595–606.
[9] S. Burke, C. Ortner, E. Süli, An Adaptive Finite Element Approximation of a Variational Model of Brittle Fracture, SIAM J. Num. Anal. , Vol. 48 (2010), p. 980-1012.
[10] R. Calhoun, M. Lowengrub, A two dimensional asymmetrical crack problem, J. Elasticity, Vol. 4 (1974), p. 37-50.
[11] B. Dacorogna, Direct Methods in the Calculus of Variations, Second Edition, Springer Verlag, New York, 2008.
[12] R.H. Dean, J.H. Schmidt, Hydraulic-Fracture Predictions with a fully coupled geomechanical reservoir simulator, SPE Journal, (2009), p. 707-714.
[13] G.A. Francfort, J.-J. Marigo, Revisiting brittle fracture as an energy minimization problem. J. Mech. Phys. Solids. 46 (8) (1998) : 1319–1342.
[14] G.A. Francfort, Un résumé de la théorie variationnelle de la rupture, Séminaire Laurent Schwartz – EDP et applications, Institut des hautes études scientifiques, 2011-2012, Exposé no. XXII, 1-11. http://slsedp.cedram.org/slsedp-bin/fitem?id=SLSEDP_2011-2012
[15] B. Ganis, V. Girault, M. Mear, G. Singh, M. F. Wheeler, Modeling fractures in a poro-elastic medium. ICES report 13-09, April 2013.
[16] Glowinski, R., Lions, J. L., TrémoliÃ¨res, R. (1976). Analyse numérique des inéquations variationnelles. Dunod.
[17] F. Irzal, J. J.C. Remmers, J. M. Huyghe, R. de Borst, A large deformation formulation for fluid flow in a progressively fracturing porous material, Comput. Methods Appl. Mech. Engrg. Vol. 256 (2013), p. 29–37.
[18] D. Kinderlehrer, G. Stampacchia, An introduction to variational inequalities and their applications. Reprint of the 1980 original. Classics in Applied Mathematics, 31. Society for Industrial and Applied Mathematics (SIAM), Philadelphia, PA, 2000. xx+313 pp.
[19] C. Miehe, F. Welschinger, M. Hofacker, Thermodynamically consistent phase-field models of fracture: variational principles and multi-field FE implementations, International Journal of Numerical Methods in Engineering, 83 (2010):1273–1311.
[20] C. Miehe, M. Hofacker, F. Welschinger, A phase field model for rate-independent crack propagation, Comput. Meth. Appl. Mech. Engrg., 199 (2010):2765–2778.
[21] A. Mikelić, M. F. Wheeler: Convergence of iterative coupling for coupled flow and geomechanics, Comput Geosci, Vol. 17 (2013), no. 3, p. 455-462. DOI 10.1007/s10596-012-9318-y.
[22] A. Mikelić , B. Wang, M. F. Wheeler, Numerical convergence study of iterative coupling for coupled flow and geomechanics, to appear in Computational Geosciences, 2014, DOI: 10.1007/s10596-013-9393-8.
[23] A. Mikelić, M. F. Wheeler, T. Wick : A phase-field approach to the fluid filled fracture surrounded by a poroelastic medium, 2013, ICES Report 13-15.
[24] A. Mikelić, M. F. Wheeler, T. Wick : A phase-field method for propagating fluid-filled fractures coupled to a surrounding porous medium, 2014, ICES Report 14-08, submitted for publication.
[25] S. Secchi and B. A. Schrefler, A method for 3-D hydraulic fracturing simulation, Int J Fract , Vol. 178 (2012), p. 245–258.
[26] I. N. Sneddon, The distribution of stress in the neighbourhood of a crack in an elastic solid, Proc. R Soc London A, Vol. 187 (1946), p. 229-60.
[27] I. N. Sneddon, M. Lowengrub, Crack problems in the classical theory of elasticity. The SIAM series in Applied Mathematics. John Wiley and Sons (1969).
[28] I. Tolstoy, ed., Acoustics, elasticity, and thermodynamics of porous media. Twenty-one papers by M.A. Biot, Acoustical Society of America, New York, 1992.
[29] M.F. Wheeler, T. Wick, W. Wollner, An augmented-Lagrangian method for the phase-field approach for pressurized fractures, Comput. Methods Appl. Mech. Engrg. 271 (2014) : 69–85.
[30] T. Wick, Solving monolithic fluid-structure interaction problems in arbitrary Lagrangian Eulerian coordinates with the deal.ii library, 2013. Archive for Numerical Software, Vol. 1, pp. 1-19, www.archnumsoft.org/
[31] T. Wick, G. Singh, M.F. Wheeler Pressurized-fracture propagation using a phase-field approach coupled to a reservoir simulator, SPE HFTC meeting in the Woodlands, SPE 168597-MS.